



Comparison among multi-chain models for entangled polymer dynamics

Journal:	<i>Soft Matter</i>
Manuscript ID	SM-ART-05-2018-000948.R1
Article Type:	Paper
Date Submitted by the Author:	04-Jun-2018
Complete List of Authors:	Masubuchi, Yuichi; Nagoya University, Department of Materials Physics Uneyama, Takashi; Nagoya University, Department of Materials Physics

Comparison among multi-chain models for entangled polymer dynamics

Yuichi Masubuchi^{1*} and Takashi Uneyama²¹Department of Materials Physics and ²Center for Computational Science, Nagoya University, Japan.

ABSTRACT

Although lots of coarse-grained models have been proposed to trace long time behaviors of entangled polymers, compatibility among the different models has not been frequently discussed. In this study, some dynamical and static quantities, such as diffusion, relaxation modulus, chain dimension, and entanglement density were examined for the multi-chain slip-link model (primitive chain network model) and the multi-chain slip-spring model, and the results were compared with those reported for the standard bead-spring model. For the diffusion, three models are compatible with scale-conversion parameters for units of length, time and, bead (segment) number (or the molecular weight). The relaxation modulus is also compatible given that the model dependence is accommodated for the entanglement density and the additional scale-conversion for the unit of modulus. The chain dimension is in reasonable coincidence with small deviations due to the weak non-Gaussianity for the models. Apart from these plausible compatibility, significant discrepancy has been found for the inter-chain cross-correlations in the relaxation modulus.

KEYWORDS

Bead-spring simulations, slip-link model, slip-spring model, viscoelasticity, multi-scale simulations

*To whom correspondence should be addressed

e-mail mas@mp.pse.nagoya-u.ac.jp

Tel +81-51-7892551

INTRODUCTION

Owing to the industrial significance as well as the scientific interest, modeling of entangled polymer dynamics has been widely attempted¹. Although molecular dynamics simulations are straightforward to trace the molecular motion, the slow relaxation nature of the system does not allow practical calculations even for coarse-grained bead-spring models². A smart idea is the single chain modeling in which multi-chain effects are embedded into motional constraints with mean-field approximations. In particular, the tube model³ and its extensions have attained remarkable success. However, the drawback of this approach is difficulties for extensions toward complex systems, which are actually targeted for molecular simulations that take account of multi-body effects explicitly.

Motivated by the situation mentioned above, several coarse-grained multi-chain models have been proposed in between bead-spring models and tube models. Such models can be classified into two categories with respect to the modeling of entanglement. The rigorous approach is to prohibit chain crossing. Padding and Briels⁴ have proposed the model referred as Twentanglement, in which the chain crossing is disallowed geometrically not relying on excluded volume interactions. A similar attempt for dissipative particle dynamics simulations⁵ has been made by introducing the segmental repulsive potential⁶. However, this straightforward direction of coarse-graining is not largely effective on the reduction of calculation costs. The other direction is to mimic the entanglement by artificial settings. The multi-chain slip-link model, so-called primitive chain network model⁷, is the realization of a network consisting of a lot of reptating chains that are bundled by slip-links in pair at the entanglements. Multi-chain slip-spring models⁸⁻¹¹ are inspired by the single-chain slip-spring model¹², in which the entanglement is reproduced by virtual springs that slide along the chain. Kindt and Briels¹³ have developed the other model so-called responsive particle dynamics to reproduce the entanglement effects by inter-particle interactions.

Although the abovementioned models have been evaluated on the basis of the comparison with experimental data, compatibility among different models is not guaranteed *a priori*, and thus comparison among the models is also necessary. Coarse-grained models cannot recover short time dynamics and small structures as a result of the smearing-out of fine scale structures, whereas finely described models such as atomistic models cannot trace long time phenomena with practical calculation costs. To overcome such difficulties, multi-scale approaches have been attempted by combining a few different molecular models¹⁴⁻¹⁷. In the multi-scale modeling, statistical consistency is assumed among the employed models in the domain where spatial and temporal scales of different models overlap with each other. In this respect, a few critical tests have been

reported for entangled polymer dynamics. Sukumaran and Likhtman¹⁸ attempted to reproduce the segmental mean-square-displacement in bead-spring simulations by the single-chain slip-spring model. They have found that in addition to the introduction of well-tuned potential between particles, the memory effect for the dynamic equation (such as the colored noise) is necessary for the single chain model rather than the usually employed memoryless dynamic equation (with the white noise), for the matching of chain dynamics. Takahashi et al¹⁹ have reported the comparison between atomistic simulations of polyethylene and bead-spring simulations for the scaling behavior of molecular weight dependence of static and dynamic measures. Their results report that the scaling behavior around the onset of entanglement is not the same. These studies reveal the applicable range of bridging between the models, as well as possibility of further improvements for coarse-grained models. Nevertheless, tests for the assumed statistical equivalence among the models are necessary.

In this study, three multi-chain models for entangled polymers are compared for the dynamics and statistics. The earlier data for the standard bead-spring model proposed by Kremer and Grest² were extracted from the literature to be compared with the results for the multi-chain slip-link model⁷ and the multi-chain slip-spring model⁸. The scale-conversion factors for length, time and bead (segment) number were determined from the diffusion behavior. With the obtained scale-conversion factors, coincidence for the relaxation modulus was confirmed. However, for the contribution of inter-chain cross-correlation in the relaxation modulus, a strong model dependence was observed. Details are shown below.

MODELS AND SIMULATIONS

In this study, multi-chain slip-link and slip-spring simulations were performed. Since the details and numerical algorithms for both models can be found in the earlier publications^{7,8,20}, a brief description is given below. In the multi-chain slip-link model (referred to as primitive chain network model PCN, hereafter), entangled polymers are replaced by a network consisting of network strands, nodes and dangling ends. Each polymer is represented by a path between two dangling ends through the strands. At each node, two polymer chains are bundled by a slip-link, which allows the chains sliding along their backbones whereas it restricts the perpendicular motions. The dynamics of the system is described by kinetic equations that take into account of the drag force from the medium, the force balance around entanglement, the osmotic force suppressing density fluctuations and the random force representing thermal agitations. When a chain penetrates out from a slip-link as a result of the sliding dynamics, the slip-link is removed and the paired chain is released. Conversely, when a chain end protrudes from a slip-link beyond a certain amount, a new

slip-link is created by hooking another segment from the surroundings. In the multi-chain slip-spring model (MCSS hereafter), multiple Rouse chains are dispersed in a simulation box. The chains are randomly connected by virtual springs (slip-springs) that mimic the entanglements. The virtual springs can slide along the chain, and they are stochastically reconstructed at the chain ends, both according to the detailed-balanced rules and the well-defined free energy.

Due to the difference in model constructions, PCN and MCSS models have different characteristic units. Naively, a conversion between different units can be achieved by scale-conversion factors. As the targets of the conversion, in this work the length, time, energy, bead (segment) number (molecular weight), and modulus are considered. For the PCN simulations, units of length, time and energy are the average segment length a_{PCN} , the diffusion time of the network node τ_{PCN} , and the thermal energy $k_B T$. τ_{PCN} is defined as $\tau_{\text{PCN}} \equiv \zeta_{\text{PCN}} a_{\text{PCN}}^2 / 6k_B T$, where ζ_{PCN} is the segment friction coefficient. For the MCSS simulations, unit of length and time is defined for a segment, with a similar manner, and denoted as a_{MCSS} and τ_{MCSS} . The unit of energy of the MCSS model is the same as the PCN model, $k_B T$.

For both models, simulations in quiescent state were performed with periodic boundary conditions. The simulation time was at least 10 times longer than the longest relaxation time for each system. The simulation box size was sufficiently larger than the chain dimension. Typically, the simulation box accommodated 800 chains for PCN simulations and 200 chains for MCSS simulations. See Appendix for the summary of actual simulated systems. For the PCN simulations, the segment number density was 10 and the osmotic parameter was 1.0 in the PCN unit mentioned above. For the MCSS simulations, the segment number density was 4 in the MCSS unit and the fugacity (activity) of slip-spring $\exp(\nu/k_B T)$ (where ν is the chemical potential for slip-springs) was 0.036. This value gives 3.5 beads between anchoring points along the chain on average. The strength parameter of slip-spring was 0.5. To improve statistical accuracy, 8 independent simulation runs starting from different initial configurations were conducted. All of these parameters and simulation conditions are essentially the same as previously reported PCN^{21,22} and MCSS^{8,23} simulations, except the entanglement density for MCSS, which is higher than that used in the previous study.

The results of simulations mentioned above were compared to literature data collected for the standard Kremer-Grest model² (KG hereafter), for which units of length and energy are the bead size σ and the energy ϵ of the Lennard-Jones potential. The unit of time τ is the standard time unit for Lennard-Jones liquids, $\tau \equiv \sigma \sqrt{m/\epsilon}$ (m is the bead mass). The bead density is 0.85 and the temperature is $k_B T = 1.0 \epsilon$. Because of this temperature, all the three models share the same

energy unit. The friction coefficient for the bead was 0.5 in the KG unit. These parameters are widely employed in the literature, and suitable for the benchmark. The static and dynamic measures discussed below will be shown in KG units unless stated.

RESULTS AND DISCUSSION

Figure 1 top panel shows the center-of-mass diffusion coefficient D as a function of bead number per chain N in the KG units. All the simulation data indicate the expected power-law like behavior, for which the power-law exponent is -1 in the unentangled regime and is roughly -2 for the large N regime beyond the onset of entanglement³. For further critical comparison, Figure 1 bottom panel shows DN^2 where the diffusion coefficient is rescaled with respect to the prediction from the classical tube theory, as proposed earlier^{12,24}. In this plot, the Rouse behavior appears as the positive slope (with the exponent of unity) and the tube behavior corresponds to a horizontal line. As reported earlier for the experimental data²⁴, the power-law exponent for diffusion coefficient with respect to the molecular weight is lower than -2 so that in Fig 1 bottom panel a negative slope appears in the large N regime, following a peak. Consequently, DN^2 shows a convex curve with respect to N , and such a behavior can be confirmed for all the models. Note that for the short chains MCSS shows the unentangled behavior in spite of the existence of slip-springs, because the dynamical constraint are not sufficiently strong to attain the entangled dynamics. For very large N , PCN and MCSS predict a plateau like behavior that hints the classical tube behavior with the exponent of -2. Although further calculations for longer chains are necessary, this behavior is consistent with some experimental data, as summarized by Likhtman¹².

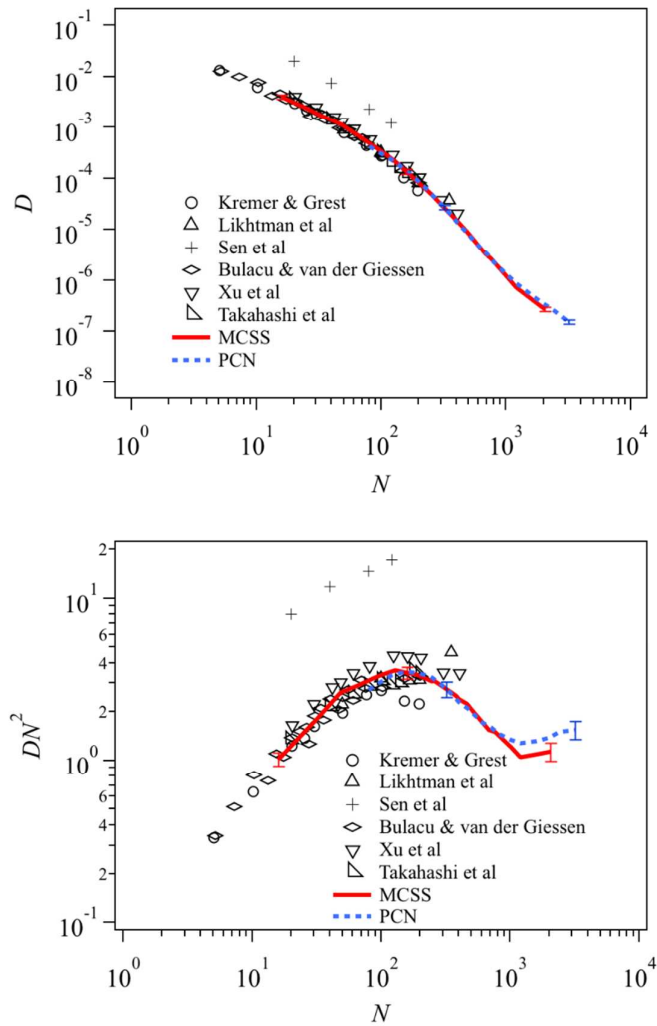


Figure 1 Center-of-mass diffusion coefficient (top) and its normalized value with respect to the classical reptation behavior (bottom) plotted against the bead number. Red solid and blue dotted curves are the results of MCSS and PCN. The MCSS and PCN data are rescaled by the scale-conversion factors. KG results obtained from the literature^{2,25-29} are shown by symbols. Error bar shows the standard deviation for 8 independent simulation runs.

Ideally, the resultant convex curve can be used for unequivocal comparison among the data. However, as shown in the figure, the bead-spring results are rather scattered for DN^2 whereas the difference is concealed in D . (For both plot, the data reported by Sen et al²⁶ are very different from the others and they seem beyond possible statistical errors by unknown reasons.) Note that the standard deviation for MCSS and PCN data obtained from 8 independent simulation runs is shown by the error-bars being smaller than the data distribution for KG. Nevertheless, the scaling factors for PCN and MCSS for the data shown in Fig 1 were thus determined by the fitting for the mean-square-displacement (MSD) for the monomers around chain center $g_1(t)$ for the chains corresponding to KG chains with $N = 50, 100, 200$ and 350 as shown in Fig 2. For PCN the short

KG chains with $N = 50$ and 100 cannot be reproduced because of the limitation of coarse-graining, as shown later. For the long chains, as described by the tube theory, $g_1(t)$ shows a series of power-law behaviors with changing the exponent with time, and the characteristic times can be determined from the transitions³. Namely, in the time scale shorter than τ_e , which is the Rouse time for the chain corresponding to the entanglement strand, the exponent is $1/2$. Between τ_e to τ_R , which is the Rouse time of the examined chain, it is $1/4$. After τ_R , the exponent becomes $1/2$ up to τ_d , which is the longest relaxation time. In the long time range beyond τ_d the exponent is unity showing the normal diffusion. These transitions have been reported for KG² as seen in Fig 2 top panel, and the transitions in the long time regime are reproduced by PCN and MCSS, although the PCN for the longest chain slightly underestimates the KG result reported by Likhtman et al²⁵. For comparison between different models with further clarity, in Fig 2 bottom panel $g_1(t)$ is multiplied by $t^{-1/2}$ as suggested by Likhtman²⁵. In this plot, the KG data reported by the other research groups are also shown, and the deviation of PCN from KG for the longest chain is within the scattering among KG data. The scattering of KG data probably indicates differences in the employed codes, initial configurations and number of chains. Nevertheless, the coincidence among different models is reasonably attained.

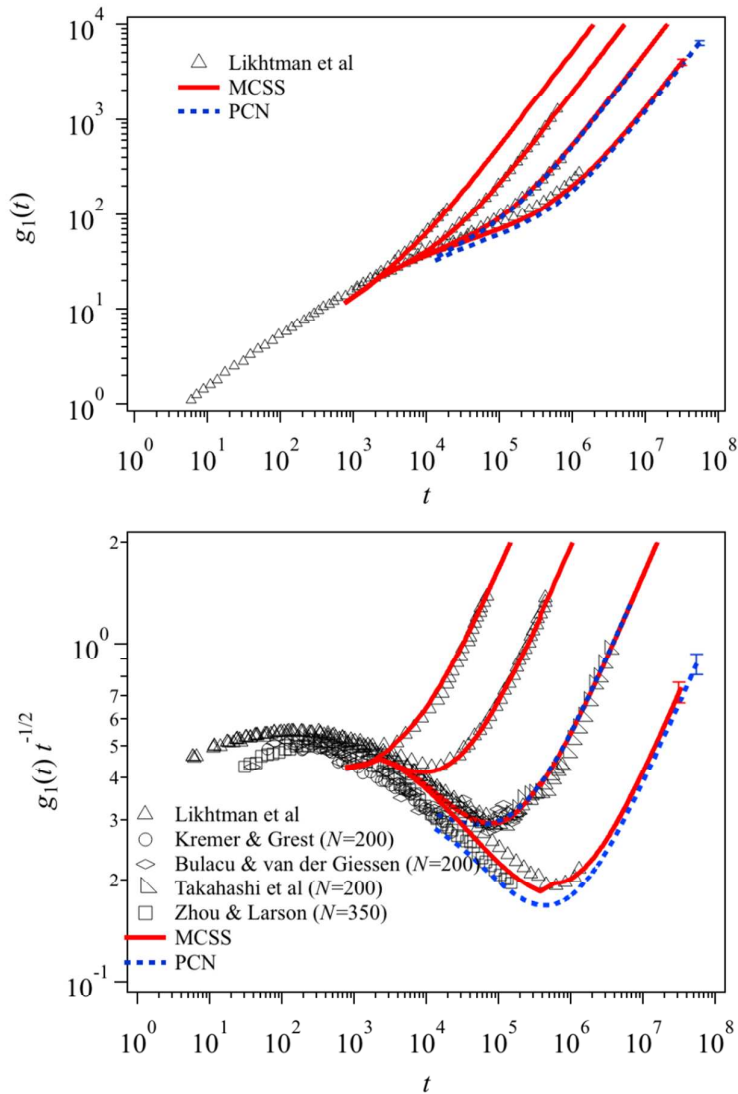


Figure 2 Time development of mean-squared-displacement of central monomers (top) and its normalized value with respect to the Rouse behavior (bottom) for $N = 50, 100, 200$ and 350 . Symbols are for KG extracted from the literature^{2,25,27,29,30}. Red solid and blue dotted curves are for MCSS and PCN. For PCN, the corresponding simulations were made for the longer KG chains with $N = 200$ and 350 . Error bar shows the standard deviation for 8 independent simulation runs.

The comparison for diffusion unequivocally determines the scaling factors for bead number, time and length. The scale-conversion factors thus determined are as follows:

$$N_{\text{PCN}} = 5N_{\text{MCSS}} = 40N \quad (1)$$

$$a_{\text{PCN}} = 2.0a_{\text{MCSS}} = 6.2\sigma \quad (2)$$

$$\tau_{\text{PCN}} = 17\tau_{\text{MCSS}} = 1.3 \times 10^4 \tau \quad (3)$$

Here, N_{PCN} and N_{MCSS} are the segment number per chain for PCN and MCSS, respectively. It is worth noting that the scale-conversion factors obtained here is different from those reported

between MCSS and KG previously⁸, due to the difference of the slip-spring density in the MCSS simulations. It is also noted that PCN simulation for the short KG chains with $N = 50$ and 100 cannot be performed, because the segment number must be integer by definition. Specifically, according to eq 1, N_{PCN} for these chains are $N_{\text{PCN}} = 1.25$ and 2.5 . The behaviors of such chains are different from those of $N_{\text{PCN}} = 2$ and 3 , for which the simulations were made.

For checking consistency between the scale-conversion factors for length and bead number, the average squared end-to-end distance $\langle \mathbf{R}^2 \rangle$ is shown in Figure 3 top panel in KG unit. Apparently there exist discrepancies among the models owing to the difference in the chain stiffness. For further clarity, in Fig 3 right panel $\langle \mathbf{R}^2 \rangle$ is divided by N . As reported earlier³¹, KG shows the non-Gaussian behavior for the short chains due to the excluded volume interaction between connected beads, indicating that the interaction is not perfectly screened. For the coarse-grained models the excluded volume interaction between segments is not directly considered and the behaviors are close to Gaussian. The deviation between KG and the other models is not negligible. Indeed, in addition to the average value of $\langle \mathbf{R}^2 \rangle$, the standard deviation shown by error-bar is different from each other. To compensate the discrepancies in chain statistics, inter-beads interactions for the coarse-grained models have to be carefully designed. For example, the interactions based on the equation of state can be utilized³². It should be also noted that the bead density must be carefully accommodated. Careful bridging attempts between atomistic molecular simulations and multi-chain slip-spring simulations have been recently reported on the basis of designed coarse-grained potentials obtained by the Boltzmann inversion scheme³³. Nevertheless, for the examined models the chain statistics is not fully consistent with the scale-conversion factors in eqs 1-3, and the scale-conversion factors would become different from those reported in eqs 1-3 if the conversion is attempted on the basis of the chain dimension rather than the diffusion.

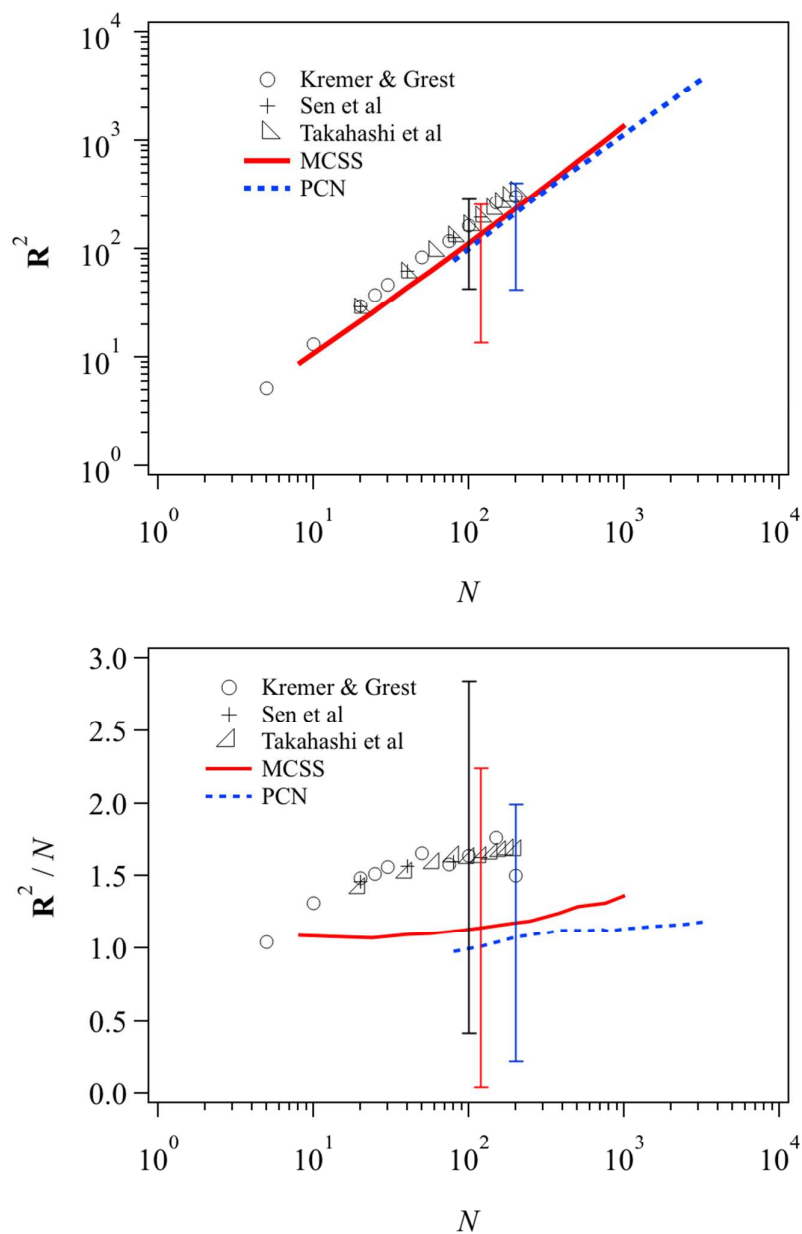


Figure 3 Squared end-to-end distance (top) and its normalized value with respect to the ideal chain statistics (bottom) plotted against bead number. Red solid and blue dotted curves are for MCSS and PCN. Symbols are for KG extracted from the literature^{2,26,29}. Error bar shows the standard deviation of the distribution for individual chains.

Although the scale-conversion parameters for relevant units have been determined from the MSD data, for rheological calculations, scale-conversion parameters for the modulus (or the scale-conversion for the stress-optical coefficient) are necessary and it must be determined from rheological response. For this sake, Figure 4 shows the comparison for linear relaxation modulus $G(t)$ obtained from the stress fluctuation by the Green-Kubo formula. In this comparison, the

temporal scale-conversion factor given by eq 3 is used, whereas the scale-conversion factor for modulus is determined to attain the best fit to the KG results reported by Likhtman et al²⁵. For further clarity for the entanglement plateau, Fig 4 right panel shows $G(t)t^{1/2}$, in which $G(t)$ is normalized with respect to the Rouse behavior. As reported earlier, the KG results for long chains clearly exhibit upward deviations from the Rouse behavior showing the effect of entanglement. These KG results are nicely reproduced by the coarse-grained models for the long chains. It is fair to note that agreement between MCSS and KG is worse than that reported in the previous study⁸. The difference is due to the choice of entanglement density, which is higher for the present study than the previous one. Consequently, the level of coarse-graining is higher and agreement for the short time behavior is worse than the previous study. Nevertheless, from the comparison, the scale-conversion parameters for modulus can be determined as follows;

$$G_{\text{PCN}} = 2.6 \times 10 G_{\text{MCSS}} = 5.2 \times 10^2 G_{\text{KG}} \quad (4)$$

One may argue that, since unit of modulus is energy per volume, the scale-conversion factors for those variables may give eq 4. However, such a conversion does not work due to the following reason. According to the rubber elasticity theory³⁴, shear modulus of polymer networks can be written as

$$G = A\nu k_{\text{B}}T = AN_{\text{e}}^{-1}nk_{\text{B}}T \quad (5)$$

Here, ν and n are the number density of network strand and segment, respectively. A is a constant depending on the network functionality and the fluctuations imposed to the network nodes³⁵⁻³⁷. N_{e} is the segment number consisting of each network strand. Because the scale-conversion factor of modulus includes the effects of A and N_{e} , it cannot be simply derived from the scale-conversion factors for energy and length. Indeed, if the modulus is compared in the same unit of length, according to the scale-conversion factor for length given by eq 2, eq 4 can be rewritten as

$$G_{\text{PCN}} = 3.2 \tilde{G}_{\text{MCSS}} = 2.2 \tilde{G}_{\text{KG}} \quad (6)$$

Here, \tilde{G}_{MCSS} and \tilde{G}_{KG} are the modulus of MCSS and KG in PCN unit. Note that the glassy contribution included in the stress of KG is not considered because eq 4 has been determined for the rubbery region.

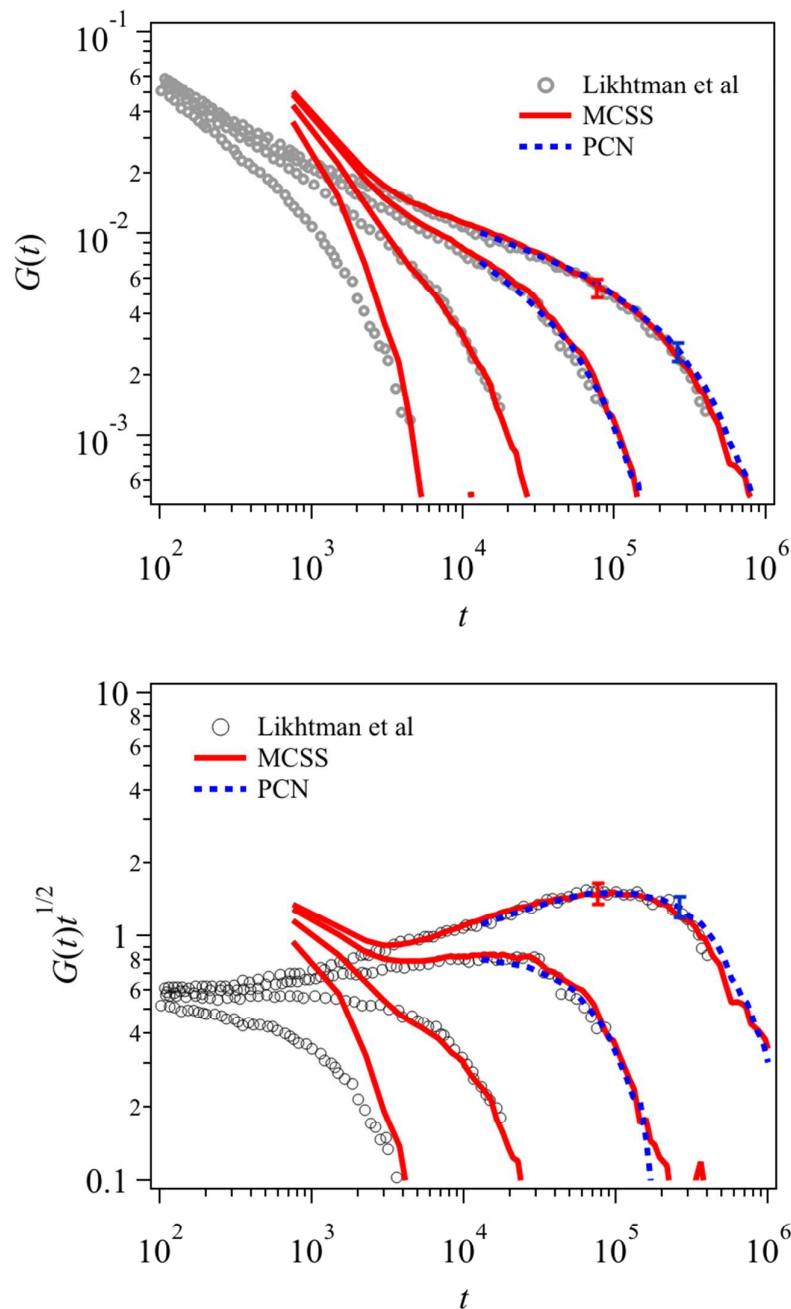


Figure 4 Linear relaxation modulus (left) and its normalized value with respect to the Rouse behavior (right) for $N = 50, 100, 200$ and 350 . Symbols are for KG results reported by Likhtman et al²⁵. Red solid and blue dotted curves are for MCSS and PCN. For PCN, the corresponding simulations were made for the longer KG chains with $N = 200$ and 350 . Error bar shows the standard deviation for 8 independent simulation runs.

As discussed above, the modulus is related to N_e , which is shown in Figure 5. For KG, several different values have been reported as summarized by Moreira et al³⁸. Kremer and Grest² estimated the bead number between entanglements from the MSD data. However, thus obtained N_e does not

coincide with the value directly calculated from the relaxation modulus³⁹. This fact means that the N_e value strongly depends on the method employed for the estimation. Recently, in most of the studies, the bead number between entanglements is reported as the Kuhn length of the primitive path, which is obtained from the primitive path analysis⁴⁰. Following the expression by Everaers⁴¹, the value obtained by this definition is referred as N_e^{PPKuhn} . N_e^{PPKuhn} increases with increasing N and saturates at $N_e^{\text{PPKuhn}} \sim 90$ for $N > 1000$. Another definition of the bead number between entanglements is the topological-based one N_e^{topo} , which is determined by the network structure obtained by Z1 code⁴² or CReTA code⁴³. Hoy et al⁴⁴ have reported N_e^{topo} of KG for various molecular weights. As seen in Fig 5, N_e^{topo} steeply decreases and reaches a steady value for $N > 100$ at $N_e^{\text{topo}} \sim 50$. Everaers⁴¹ proposed the relation between N_e^{PPKuhn} and N_e^{topo} , and for the binary assumption of entanglement $N_e^{\text{PPKuhn}} = 2N_e^{\text{topo}}$, which is roughly consistent with Fig 5. Nevertheless, as discussed by Everaers⁴¹, the networks in the slip-link and slip-spring models are topological-based and to be compared with N_e^{topo} .

Because the entanglement is introduced *a priori* for MCSS and PCN, N_e for these models can be obtained from the actual density of slip-springs and slip-links and the scale-conversion factor for the segment number given by eq 1. The N_e^{topo} thus obtained for MCSS and PCN are plotted in Figure 5 by red solid and blue dotted curves, respectively. Figure 5 demonstrates that N_e^{topo} is model dependent, and the bridging among the models cannot be attained from a naive structural mapping for the entanglement network. Indeed, the entanglement density defined as $\nu \equiv n/N_e$ is model dependent. From the scale-conversion factor of length given by eq 2, the segment density of each model, and N_e^{topo} shown in Fig 5, the relation of density for the entanglement strands among the different models is written as

$$\nu_{\text{PCN}} = \tilde{\nu}_{\text{MCSS}} = 2.2\tilde{\nu}_{\text{KG}} \quad (7)$$

Here $\tilde{\nu}_{\text{MCSS}}$ and $\tilde{\nu}_{\text{KG}}$ are the strand density of MCSS and KG with respect to the unit volume of PCN. The other reason for the difference of N_e^{topo} is the imposed fluctuations around the entanglement. The magnitude of fluctuations can be discussed by the constant A in eq 5. From eqs 4-6, the relation among A can be written as

$$A_{\text{PCN}} = 3.2 A_{\text{MCSS}} = A_{\text{KG}} \quad (8)$$

Interestingly, this relation suggests that the magnitude of fluctuations for PCN is close to that for KG, whereas for MCSS it is larger than the other models. For PCN and MCSS, the magnitude of fluctuations is specified *a priori*, whereas for KG the fluctuations are of difficult evaluation for the extracted frozen topological network⁴⁵. Because for PCN and MCSS the fluctuations are controlled by the parameters related to the dynamics of slip-links and slip-springs, tuning of such parameters^{32,33} would be necessary as well as the tuning of structural parameters for further discussion. It is also noted that for the entanglement structure, the distributions for N_e^{topo} must be

discussed in addition to its average value. Although the consistency for PCN and MCSS with atomistic simulations has been reported^{46,47}, distributions for the standard KG simulations have not been reported in our knowledge and no comparison can be made at this time being.

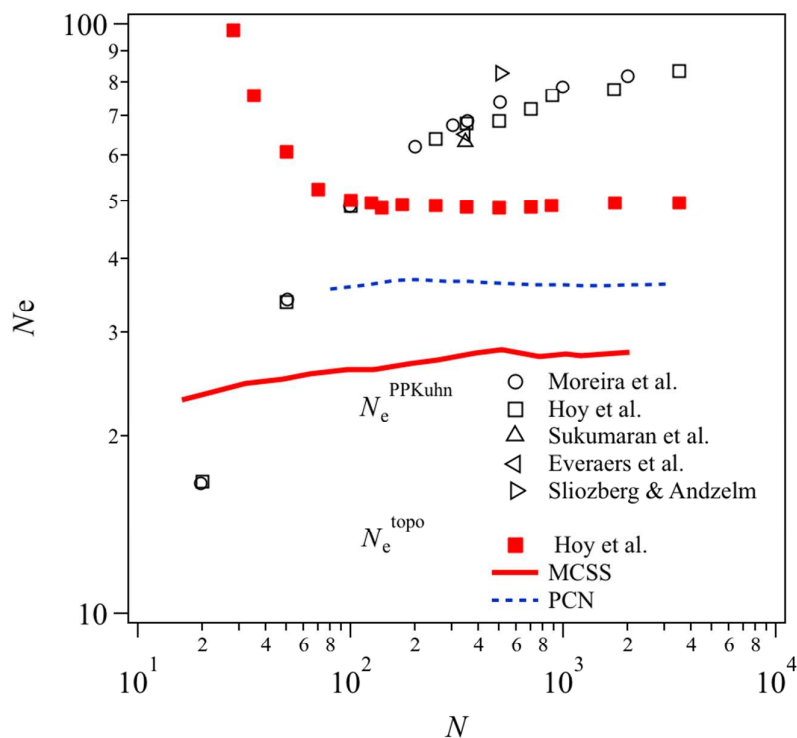


Figure 5 Bead number between entanglements N_e plotted against bead number per chain. Red solid and blue dotted curves are for MCSS and PCN. Symbols are KG results from the literature^{38,40,44,48,49}, and filled and unfilled ones are for N_e^{topo} and N_e^{PPKuhn} , respectively.

For the comparison among the models, the inter-chain cross-correlation is an interesting issue⁵⁰. Although the chain dynamics is assumed to be independent in the single chain modeling, multi-chain models have shown non-negligible amount of cross-correlations. Indeed, for KG, the cross-correlation has been discussed from a few different approaches^{25,51–53}. In this specific study, the coupling parameter introduced by Cao and Likhtman⁵³ is discussed. The coupling parameter $\kappa(t)$ is the ratio of cross-correlation contribution to the entire relaxation modulus. Recalling the success of single chain models, one may suppose that $\kappa(t)$ is close to zero or rapidly relaxes. However, $\kappa(t)$ grows with time and reaches ca. 50% of the total relaxation modulus for KG, as shown in Fig 6. For the coarse-grained models, growth of $\kappa(t)$ is also observed⁵⁴, including the upturn around the terminal time. However, the magnitude depends on the model and no universality is found here. Because the coupling between chains strongly depends on the interaction between

beads or segments, rather short-range interactions such as the Lennard-Jones potential and the compressibility parameter would affect the behavior of the coupling parameter. Masubuchi and Amamoto⁵⁵ have shown that the magnitude of $\kappa(t)$ slightly depends on the incompressibility for PCN. Their result suggests that the tuning of inter-beads interactions for the coarse-grained models would compensate the discrepancy in $\kappa(t)$. However, such a modification for the models may disturb the consistencies for the other dynamical measures. Nevertheless, further investigation for $\kappa(t)$ is apparently necessary.

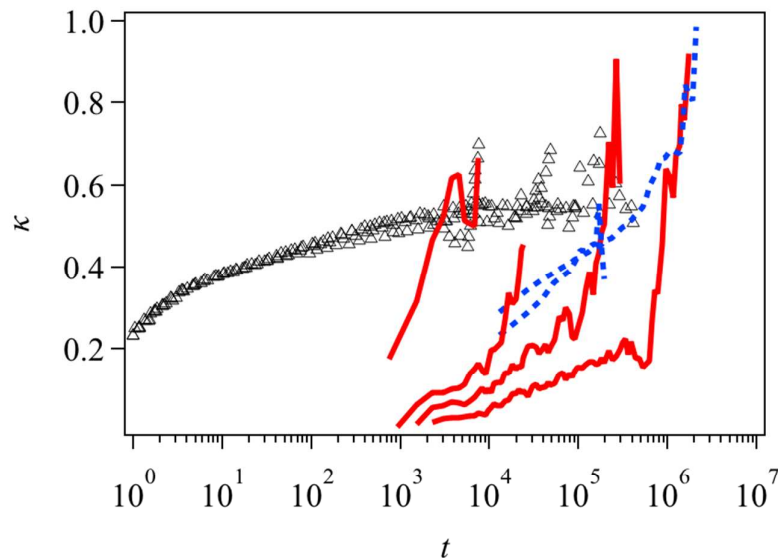


Figure 6 Time development of coupling parameter for inter-chain cross-correlations for $N = 50, 100, 200$ and 350 . Red solid and blue dotted curves are for MCSS and PCN. Symbols are for KG results reported by Cao and Likhtman⁵³. For PCN, the corresponding simulations were made for the longer KG chains with $N = 200$ and 350 .

CONCLUSIONS

Detailed comparison has been performed among multi-chain models for dynamical and static measures for entangled polymers. As reported earlier, all the models nicely exhibit the established universal behaviors for dynamical measures such as diffusion and relaxation modulus. Owing to the universality, the scale-conversion factors have been reasonably determined for time, length, bead (segment) number and modulus. For chain dimensions, small inconsistencies have been observed due to the weak non-Gaussian nature of KG and the lack of tunings for the inter-segment interactions in the coarse-grained models. Apart from the plausible results mentioned above, non-universal behaviors have been found for the inter-chain cross-correlation for the relaxation modulus.

The results of this study confirm applicability of multi-scale strategies that rely on the universality of dynamic and static measures for entangled polymers. In particular, for the dynamical measures coincidence is attainable even without detailed tuning for the model parameters. Meanwhile, it has been revealed that the significant inconsistency for the inter-chain cross-correlation is concealed. Because inter-chain cross-correlations are difficult measure for experiments, further studies are apparently necessary for different multi-chain models. The other issue to be clarified is the compatibilities among the models under strong deformations and flows. Studies in such directions are being conducted and the results will be published elsewhere.

APPENDIX

The simulated conditions for MCSS and PCN are summarized in Table I shown below. The molecular weight is shown in the unit of each model. Namely, for MCSS it corresponds to the Rouse bead number per chain whereas for PCN it stands for the average number of entanglement strands per chain. The unit cell dimension is also shown in the length unit of each model. Note that, as mentioned in the text, 8 independent simulation runs starting from different initial configurations were performed for each condition.

Table I. Simulated conditions for MCSS and PCN.

Model	Molecular weight	Chain number	Cell dimension
MCSS	2	200	4.64
	3	200	5.31
	4	200	5.85
	6	200	6.69
	8	200	7.37
	12	200	8.43
	16	200	9.28
	20	200	10.00
	24	200	10.62
	31	200	11.57
	32	200	11.70
	44	200	13.01
	48	200	13.39
	50	200	13.57
	58	200	14.26
	64	200	14.74
	85	200	16.19
96	200	16.87	
128	200	18.57	
150	300	22.41	
196	300	24.49	
256	500	31.75	
PCN	2	2560	8

3	1707	8
4	1280	8
5	1024	8
6	853	8
7	731	8
8	640	8
9	1111	10
10	1000	10
12	833	10
15	667	10
18	556	10
20	500	10
25	691	12
30	576	12
40	843	15
50	676	15
60	562	15
80	422	15

ACKNOWLEDGEMENT

This study is supported in part by Grant-in-Aid for Scientific Research (A) (17H01152) and for Scientific Research on Innovative Areas (18H04483) from JSPS. The support is also made by Council for Science, Technology and Innovation, Cross-ministerial Strategic Innovation Promotion Program, “Structural Materials for Innovation” from JST.

REFERENCES

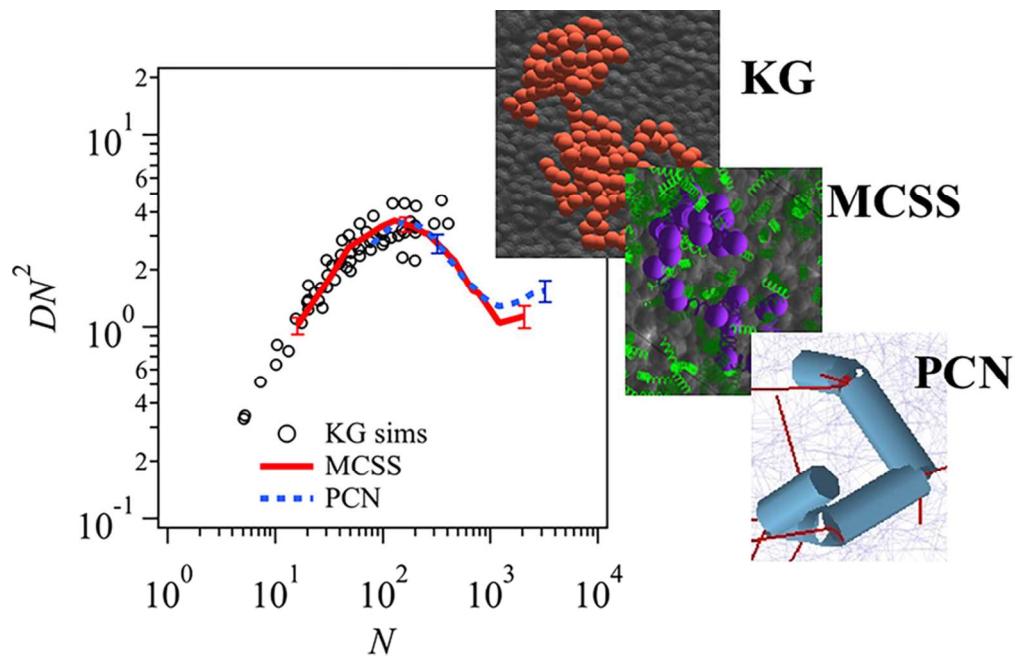
- 1 Y. Masubuchi, Simulating the Flow of Entangled Polymers, *Annu. Rev. Chem. Biomol. Eng.*, 2014, **5**, 11–33.
- 2 K. Kremer and G. S. Grest, Dynamics of entangled linear polymer melts: A molecular-dynamics simulation, *J. Chem. Phys.*, 1990, **92**, 5057.
- 3 M. Doi and S. F. Edwards, *The Theory of Polymer Dynamics*, Clarendon press, Oxford, 1986.
- 4 J. T. Padding and W. J. Briels, Uncrossability constraints in mesoscopic polymer melt simulations: Non-Rouse behavior of C[_{sub 120}]H[_{sub 242}], *J. Chem. Phys.*, 2001, **115**, 2846.
- 5 F. Lahmar, C. Tzoumanekas, D. N. Theodorou and B. Rousseau, Onset of Entanglements Revisited. Dynamical Analysis, *Macromolecules*, 2009, **42**, 7485–7494.
- 6 S. Kumar and R. G. Larson, Brownian dynamics simulations of flexible polymers with spring–spring repulsions, *J. Chem. Phys.*, 2001, **114**, 6937.
- 7 Y. Masubuchi, J.-I. Takimoto, K. Koyama, G. Ianniruberto, G. Marrucci and F. Greco,

- Brownian simulations of a network of reptating primitive chains, *J. Chem. Phys.*, 2001, **115**, 4387.
- 8 T. Uneyama and Y. Masubuchi, Multi-chain slip-spring model for entangled polymer dynamics, *J. Chem. Phys.*, 2012, **137**, 154902.
- 9 V. C. Chappa, D. C. Morse, A. Zippelius and M. Müller, Translationally Invariant Slip-Spring Model for Entangled Polymer Dynamics, *Phys. Rev. Lett.*, 2012, **109**, 148302.
- 10 A. Ramírez-Hernández, F. A. Detcheverry, B. L. Peters, V. C. Chappa, K. S. Schweizer, M. Müller and J. J. de Pablo, Dynamical Simulations of Coarse Grain Polymeric Systems: Rouse and Entangled Dynamics, *Macromolecules*, 2013, **46**, 6287–6299.
- 11 M. Langeloth, Y. Masubuchi, M. C. Böhm and F. Müller-plathe, Recovering the reptation dynamics of polymer melts in dissipative particle dynamics simulations via slip-springs., *J. Chem. Phys.*, 2013, **138**, 104907.
- 12 A. E. Likhtman, Single-chain slip-link model of entangled polymers: simultaneous description of neutron spin-echo, rheology, and diffusion, *Macromolecules*, 2005, **38**, 6128–6139.
- 13 P. Kindt and W. J. Briels, A single particle model to simulate the dynamics of entangled polymer melts, *J. Chem. Phys.*, 2007, **127**, 134901.
- 14 K. Kremer and F. Müller-Plathe, Multiscale Problems in Polymer Science: Simulation Approaches, *MRS Bull.*, 2001, **26**, 205–210.
- 15 F. Müller-Plathe, Coarse-Graining in Polymer Simulation: From the Atomistic to the Mesoscopic Scale and Back, *ChemPhysChem*, 2002, **3**, 754–769.
- 16 V. A. Harmandaris, N. P. Adhikari, N. F. A. Van Der Vegt and K. Kremer, Hierarchical modeling of polystyrene: From atomistic to coarse-grained simulations, *Macromolecules*, 2006, **39**, 6708–6719.
- 17 P. S. Stephanou, C. Baig and V. G. Mavrantzas, Projection of atomistic simulation data for the dynamics of entangled polymers onto the tube theory: calculation of the segment survival probability function and comparison with modern tube models, *Soft Matter*, 2011, **7**, 380–395.
- 18 S. K. Sukumaran and A. E. Likhtman, Modeling entangled dynamics: Comparison between stochastic single-chain and multichain models, *Macromolecules*, 2009, **42**, 4300–4309.
- 19 K. Z. Takahashi, R. Nishimura, N. Yamato, K. Yasuoka and Y. Masubuchi, Onset of static and dynamic universality among molecular models of polymers, *Sci. Rep.*, 2017, **7**, 12379.
- 20 Y. Masubuchi, G. Ianniruberto, F. Greco and G. Marrucci, Molecular simulations of the long-time behaviour of entangled polymeric liquids by the primitive chain network model, *Model. Simul. Mater. Sci. Eng.*, 2004, **12**, S91–S100.
- 21 Y. Masubuchi and Y. Amamoto, Orientational Cross-Correlation in Entangled Binary Blends

- in Primitive Chain Network Simulations, *Macromolecules*, 2016, **49**, 9258–9265.
- 22 Y. Masubuchi, A. Pandey, Y. Amamoto and T. Uneyama, Orientational cross correlations between entangled branch polymers in primitive chain network simulations, *J. Chem. Phys.*, 2017, **147**, 184903.
- 23 Y. Masubuchi, Effects of degree of freedom below entanglement segment on relaxation of polymer configuration under fast shear in multi-chain slip-spring simulations, *J. Chem. Phys.*, 2015, **143**, 224905.
- 24 T. P. Lodge, Reconciliation of the molecular weight dependence of diffusion and viscosity in entangled polymers, *Phys. Rev. Lett.*, 1999, **83**, 3218–3221.
- 25 A. E. Likhtman, S. K. Sukumaran and J. Ramirez, Linear Viscoelasticity from Molecular Dynamics Simulation of Entangled Polymers, *Macromolecules*, 2007, **40**, 6748–6757.
- 26 S. Sen, S. K. Kumar and P. Koblinski, Viscoelastic Properties of Polymer Melts from Equilibrium Molecular Dynamics Simulations, *Macromolecules*, 2005, **38**, 650–653.
- 27 M. Bulacu and E. van der Giessen, Effect of bending and torsion rigidity on self-diffusion in polymer melts: A molecular-dynamics study, *J. Chem. Phys.*, 2005, **123**, 114901.
- 28 X. Xu, J. Chen and L. An, Simulation studies on architecture dependence of unentangled polymer melts, *J. Chem. Phys.*, 2015, **142**, 074903.
- 29 K. Z. Takahashi, N. Yamato, K. Yasuoka and Y. Masubuchi, Critical test of bead–spring model to resolve the scaling laws of polymer melts: a molecular dynamics study, *Mol. Simul.*, 2017, **43**, 1196–1201.
- 30 Q. Zhou and R. G. Larson, Direct molecular dynamics simulation of branch point motion in asymmetric star polymer melts, *Macromolecules*, 2007, **40**, 3443–3449.
- 31 R. Auhl, R. Everaers, G. S. Grest, K. Kremer and S. J. Plimpton, Equilibration of long chain polymer melts in computer simulations, *J. Chem. Phys.*, 2003, **119**, 12718.
- 32 G. G. Vogiatzis, G. Megariotis and D. N. Theodorou, Equation of State Based Slip Spring Model for Entangled Polymer Dynamics, *Macromolecules*, 2017, **50**, 3004–3029.
- 33 A. P. Sgouros, G. Megariotis and D. N. Theodorou, Slip-Spring Model for the Linear and Nonlinear Viscoelastic Properties of Molten Polyethylene Derived from Atomistic Simulations, *Macromolecules*, 2017, **50**, 4524–4541.
- 34 P. J. Flory, *Principles of polymer chemistry*, Cornell University Press, Ithaca, New York, 1953.
- 35 R. Everaers, Entanglement effects in defect-free model polymer networks, *New J. Phys.*, 1999, **1**, 12.1-12.54.
- 36 Y. Masubuchi, G. Ianniruberto, F. Greco and G. Marrucci, Entanglement molecular weight and frequency response of sliplink networks, *J. Chem. Phys.*, 2003, **119**, 6925–6930.
- 37 R. G. Larson, T. Sridhar, L. G. Leal, G. H. McKinley, A. E. Likhtman and T. C. B. McLeish,

- Definitions of entanglement spacing and time constants in the tube model, *J. Rheol. (N. Y. N. Y.)*, 2003, **47**, 809.
- 38 L. A. Moreira, G. Zhang, F. Müller, T. Stuehn and K. Kremer, Direct Equilibration and Characterization of Polymer Melts for Computer Simulations, *Macromol. Theory Simulations*, 2015, **24**, 419–431.
- 39 M. Pütz, K. Kremer and G. S. Grest, What is the entanglement length in a polymer melt?, *Europhys. Lett.*, 2000, **49**, 735–741.
- 40 R. Everaers, S. K. Sukumaran, G. S. Grest, C. Svaneborg, A. Sivasubramanian and K. Kremer, Rheology and microscopic topology of entangled polymeric liquids., *Science (80-.)*, 2004, **303**, 823–826.
- 41 R. Everaers, Topological versus rheological entanglement length in primitive-path analysis protocols, tube models, and slip-link models, *Phys. Rev. E - Stat. Nonlinear, Soft Matter Phys.*, 2012, **86**, 1–5.
- 42 M. Kroger, Shortest multiple disconnected path for the analysis of entanglements in two- and three-dimensional polymeric systems, *Comput. Phys. Commun.*, 2005, **168**, 209–232.
- 43 C. Tzoumanekas and D. N. Theodorou, Topological analysis of linear polymer melts: a statistical approach, *Macromolecules*, 2006, **39**, 4592–4604.
- 44 R. S. Hoy, K. Foteinopoulou and M. Kröger, Topological analysis of polymeric melts: Chain-length effects and fast-converging estimators for entanglement length, *Phys. Rev. E - Stat. Nonlinear, Soft Matter Phys.*, 2009, **80**, 14–16.
- 45 W. Bisbee, J. Qin and S. T. Milner, Finding the tube with isoconfigurational averaging, *Macromolecules*, 2011, **44**, 8972–8980.
- 46 Y. Masubuchi, T. Uneyama, H. Watanabe, G. Ianniruberto, F. Greco and G. Marrucci, Structure of entangled polymer network from primitive chain network simulations, *J. Chem. Phys.*, 2010, **132**, 1–8.
- 47 A. Ramírez-Hernández, B. L. Peters, M. Andreev, J. D. Schieber and J. J. de Pablo, A multichain polymer slip-spring model with fluctuating number of entanglements for linear and nonlinear rheology, *J. Chem. Phys.*, 2015, **143**, 243147.
- 48 S. K. Sukumaran, G. S. Grest, K. Kremer and R. Everaers, Identifying the primitive path mesh in entangled polymer liquids, *J. Polym. Sci. Part B Polym. Phys.*, 2005, **43**, 917–933.
- 49 Y. R. Sliozberg and J. W. Andzelm, Fast protocol for equilibration of entangled and branched polymer chains, *Chem. Phys. Lett.*, 2012, **523**, 139–143.
- 50 A. E. Likhtman, Whither tube theory: From believing to measuring, *J. Nonnewton. Fluid Mech.*, 2009, **157**, 158–161.
- 51 J. Gao and J. H. Weiner, Contribution of covalent bond force to pressure in polymer melts, *J. Chem. Phys.*, 1989, **91**, 3168.

- 52 J. Ramírez, S. K. Sukumaran and A. E. Likhtman, Significance of cross correlations in the stress relaxation of polymer melts, *J. Chem. Phys.*, 2007, **126**, 244904.
- 53 J. Cao and A. E. Likhtman, Time-dependent orientation coupling in equilibrium polymer melts, *Phys. Rev. Lett.*, 2010, **104**, 207801.
- 54 Y. Masubuchi and S. K. Sukumaran, Cross-Correlation Contributions to Orientational Relaxations in Primitive Chain Network Simulations, *Nihon Reoroji Gakkaishi*, 2013, **41**, 1–6.
- 55 Y. Masubuchi and Y. Amamoto, Effect of Osmotic Force on Orientational Cross-correlation in Primitive Chain Network Simulation, *Nihon Reoroji Gakkaishi*, 2016, **44**, 219–222.



77x49mm (300 x 300 DPI)